I&EC research
Industrial & Engineering Chemistry Research

pubs.acs.org/IECR

Article

Kinetics and Reactor Design Principles of Volatile Fatty Acid Ketonization for Sustainable Aviation Fuel Production

Jacob H. Miller, Glenn R. Hafenstine, Hannah H. Nguyen, and Derek R. Vardon*

Cite This: *Ind. Eng. Chem. Res.* 2022, 61, 2997−3010

Read Online

ACCESS | Metrics & More | Article Recommendations | Supporting Information

ABSTRACT: Ketonization of wet waste-derived carboxylic acids (volatile fatty acids, VFAs) constitutes the first step of a process to catalytically upgrade VFAs to an alkane sustainable aviation fuel blendstock. VFA ketonization has been demonstrated at near-theoretical yields at the lab scale, and robust operation of industrial-scale ketonization reactors is essential for the commercialization of VFA upgrading to sustainable aviation fuel. We present a ketonization kinetic study of hexanoic acid, a VFA model compound, over commercial ZrO_2 and use the kinetic parameters derived from the study in an adiabatic packed-bed reactor simulation of hexanoic acid ketonization running to near-complete (98%) conversion. A key findings from the kinetic study is that ketonization rate is positive order in acid pressure at low (<10 kPa) pressures and transitions to zero order at higher pressures, conforming to a Langmuir−Hinshelwood surface coupling mechanism. Rates are inhibited by ketonization coproduct water but not by ketones themselves or coproduct CO_2. Reactor simulations using these kinetics show that rate inhibition by water controls reactor size and that size requirements can be lessened by employing designs that allow for the removal of water from the partially converted acid stream.

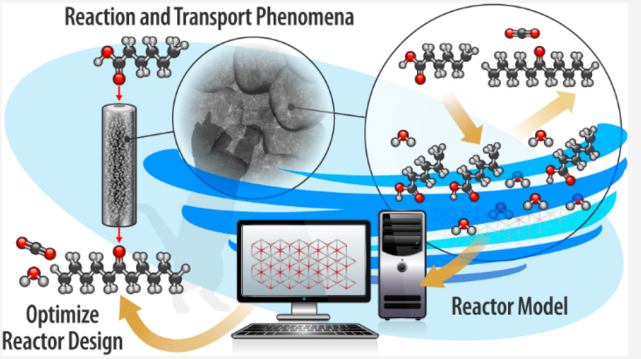

1. INTRODUCTION

The accelerating pace and scale of climate change consequences stemming from anthropogenic greenhouse gas emissions emphasizes the need for decarbonization of fossil fuel-reliant industries.[1] Aviation accounts for 2.5% of global greenhouse gas emissions[2] and the most promising near-term strategies for advancing aviation sustainability are through development of biomass-derived aviation fuels from abundant and inexpensive biomass sources.[3] Volatile fatty acids (VFAs, C_{2-8} carboxylic acids) generated from wet wastes such as food waste, animal manure, and wastewater sludge are a potential sustainable aviation fuel feedstock.[4,5] Anaerobic digestion of wet wastes by microbial consortia normally forms CO_2 and CH_4 but can be altered to instead produce VFAs via arrested methanogenesis.[6−8] Biomass conversion pathways to aviation fuel have been collectively termed "sustainable," but quantifying the carbon intensity of such approaches to ensure sufficient reductions compared to fossil fuel use is necessary to completely assess the benefits of each pathway.[9] Recent life cycle analysis of the pathway studied in this work, VFA upgrading to sustainable aviation fuel (SAF) via sequential ketonization and hydrotreating, found that the process has a carbon emissions intensity below zero (−55 g CO_{2eq} MJ^{-1}) due to avoided methane emissions otherwise generated when wet waste is landfilled.[10] Life-cycle analyses of VFA upgrading to diesel blendstocks[11] and fatty acid upgrading to waxes[12] and surfactants[13] also show that valorization of waste acids for fuels and chemicals results in substantial carbon intensity reductions. Thus, upgrading of wet waste-derived VFAs for use as aviation fuel blendstocks is a promising decarbonization pathway.

Aviation fuel must contain a mixture of hydrocarbons with varying functionalities (*n*-alkanes, cyclic alkanes, branched alkanes, and aromatics) to meet specifications for key operability properties such as boiling behavior, freezing point, viscosity, and flash point.[14,15] N-alkanes comprise a significant amount (20%) of fossil aviation fuel[14] and are thus an important component for inclusion in SAF. Carbon chain lengths between 9 and 15 are particularly desirable for *n*-alkanes, as blends of these alkanes in aviation fuel meet freezing point, flash point, and viscosity specifications, unlike shorter- or longer-chain *n*-alkanes, because the carbon chain length distribution in aviation fuel is centered around 11.[10] VFAs can be transformed into *n*-alkanes via catalytic ketonization and subsequent ketone hydrodeoxygenation.[10,16] Derisking of the catalytic VFA ketonization step is a critical

Received: December 1, 2021
Revised: February 9, 2022
Accepted: February 9, 2022
Published: February 18, 2022

https://doi.org/10.1021/acs.iecr.1c04548
Ind. Eng. Chem. Res. 2022, 61, 2997−3010

Scheme 1. Strategy to Understand VFA Ketonization Kinetics and Optimize Design of a Packed-Bed VFA Ketonization Reactor

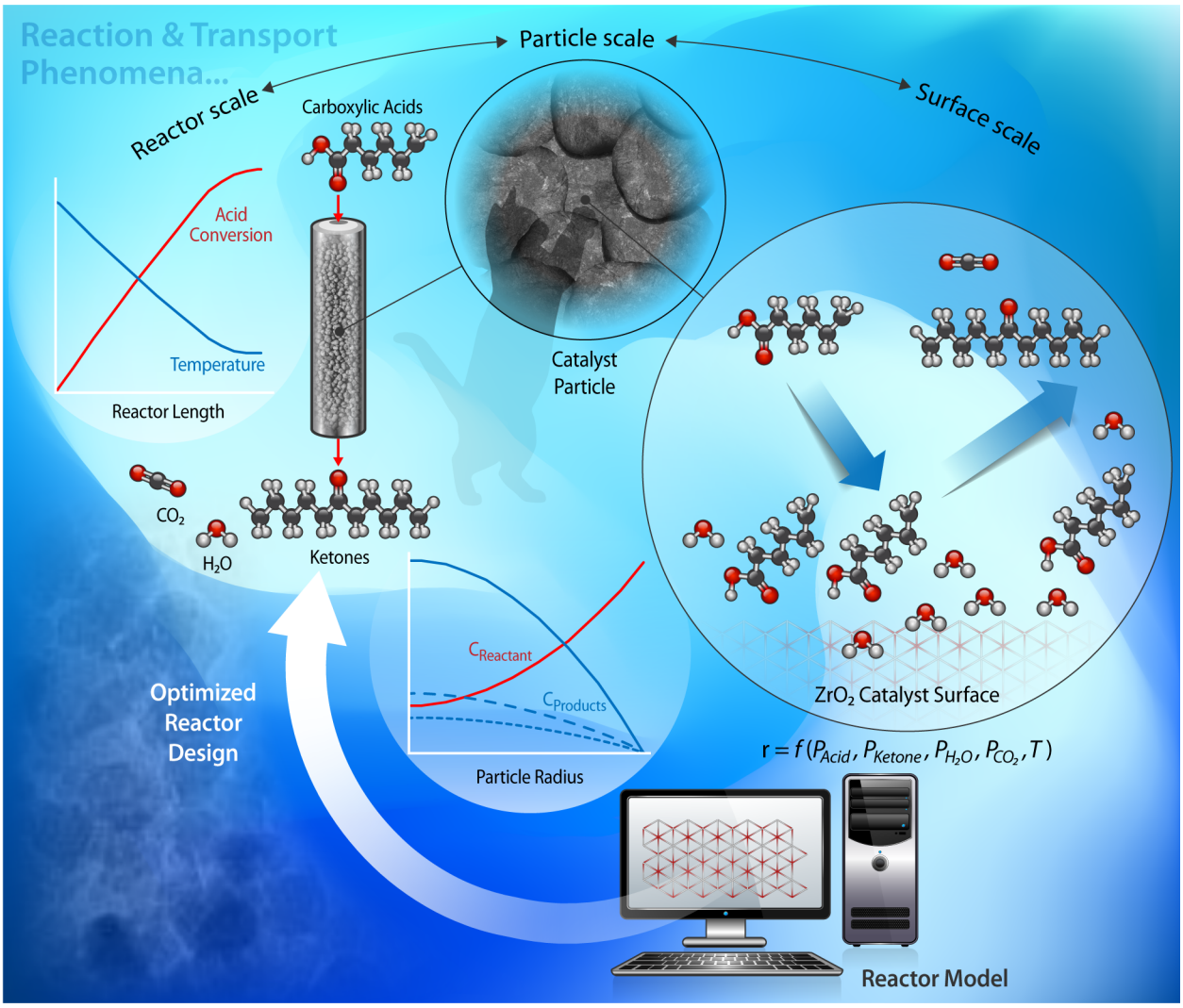

priority because ketonization is not currently performed industrially, whereas hydrodeoxygenation has been implemented at an industrial scale for production of fuels derived from fats, oils, and greases,[17] which have similar oxygen content to ketones. Ketonization involves coupling of two carboxylic acids to produce one ketone, along with single molecules of CO_2 and water (Scheme 1). Ketonization of vapor-phase VFAs has been observed over a range of solid acid catalysts possessing either Lewis and Brønsted acidity,[18−21] although ZrO_2 and TiO_2 have specifically attracted a great deal of attention because of their low price and high abundance.[22−28] Albrecht and colleagues[29−31] also studied ketonization of condensed aqueous-phase propionic and acetic acids. Near-theoretical yields of ketones have been obtained in vapor-phase packed-bed reactors over solid acid catalysts from biogenically derived C_{2-8} VFAs,[10] propionic acid,[32,33] and acetic acid,[24] suggesting that this process is viable. Deactivation of catalysts with time on stream has been observed by Almutairi et al.[34] in a study of acetic acid ketonization over several oxides and Lee et al.[35] in a study of C_{16-18} acid ketonization over TiO_2. Almutairi et al.[34] and Lee et al.[35] both directly correlated deactivation to surface coke accumulation and Almutairi et al. demonstrated that air treatment of catalysts was an effective technique to reverse the effects of deactivation. The high ketonization conversions and selectivities achieved on the lab scale and demonstrations of catalyst regenerability suggest that this process has the potential to be successfully scaled up with currently available catalysts.

Kinetic models for ketonization of VFAs over solid acids have been formulated by Pham et al.,[25,36] Gärtner et al.,[26,37,38] Wang and Iglesia,[27] and Shylesh et al.[39] These studies concur that ketonization over solid acids occurs via a kinetically relevant bimolecular coupling step involving acid and/or base sites over Ru/TiO_2, TiO_2, CeO_2-ZrO_2, and Zr/SiO_2 powders. The kinetic models fit by these authors[25−27,36−39] explain observed trends in rate with reactant pressures; Pham et al., Gärtner et al., and Shylesh et al. also incorporate inhibition of rates by ketonization products. Wang and Iglesia[27] observed production of acid anhydrides as a ketonization side product and performed thermodynamic analysis to show that anhydrides are equilibrated with carboxylic acids during ketonization over oxides (Scheme 2, bottom left arrow). Most ketonization mechanisms over oxide catalysts such as those proposed by Pham et al.[25,36] and Wang and Iglesia[27] based on kinetic studies and Pulido et al.[40] and Shylesh et al.[39] based on combinations of kinetic studies and density

https://doi.org/10.1021/acs.iecr.1c04548
Ind. Eng. Chem. Res. 2022, 61, 2997−3010

Scheme 2. Hexanoic Acid Ketonization to 6-Undecanone, Water, and CO_2 with an Equilibrated Side Reaction Producing Hexanoic Anhydride and Water

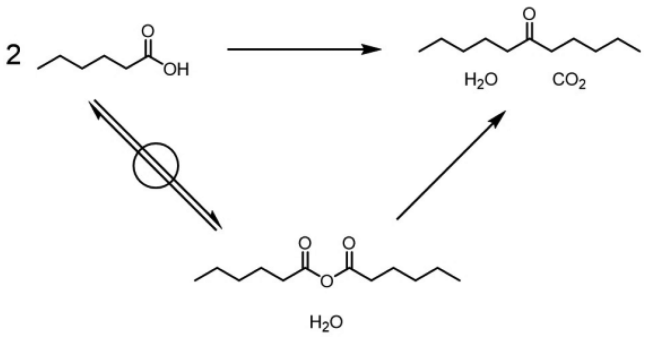

functional theory calculations do not involve anhydrides, but the ketonization mechanism proposed by Bamberger[41,42] does invoke an anhydride intermediate. Informed design of ketonization reactors requires robust kinetic models such as these, which accurately quantify the effects of reactant and product concentrations, as well as temperature, on reaction rates.

In this work, we conduct a kinetic study of ketonization of a model compound, hexanoic acid, and fit our observed data to a kinetic model, which we implement to simulate an industrial-scale ketonization reactor and develop recommendations for commercial-scale reactor designs (Scheme 1). Hexanoic acid was chosen as a model compound because the carbon number of 6-undecanone, the self-ketonization product of this hexanoic acid (11), is close to the average carbon number of fossil jet fuel (11.4).[10,14] We estimate kinetic parameters governing ketonization over commercial ZrO_2 (extrudates ground into powder) from packed-bed reactor kinetics experiments conducted at differential conversion at conditions free of mass and heat transfer limitations. Results of the kinetic study, described quantitatively by a Langmuir−Hinshelwood model, indicate that hexanoic acid saturates the ZrO_2 surface at ∼10 kPa and that rates are independent of acid concentration at higher pressures and that, of the ketonization products, only water inhibits rates. Our packed-bed reactor model simulates ketonization over extrudates of the same commercial ZrO_2 extrudates used in powder form for kinetic studies and incorporates intraparticle diffusion limitations and axial pressure drop. We identify rate inhibition by water as the principal driver of reactor size and demonstrate that reactor configurations allowing for the removal of water before achievement of near-complete (98%) acid conversion decreases the necessary reactor size and pressure drop.

2. EXPERIMENTAL SECTION

2.1. Reaction Kinetics Experimental Methods. Hexanoic acid (≥99%, Sigma-Aldrich) and isopentanoic acid (99%, Sigma-Aldrich) ketonization flow reactions were performed while 6-undecanone (98%, TCI America), CO_2 (General Air), and deionized water were cofed. Helium (Matheson Gas, 99.999%) was used as a sweep gas. ZrO_2 particles used as ketonization catalysts were obtained from Johnson-Matthey (CP836 extrudates; 3.16 mm diameter and 5.44 mm length), crushed to 149−177 μm particle size (80−100 mesh), and heat-treated at 550 °C in stagnant air prior to use. Surface area and pore size distribution were measured by N_2 physisorption using a Quantachrome Instruments Autosorb-1. Specific BET surface area of the ZrO_2 was 74.2 $m^2\ g^{-1}$ and the average pore radius was determined to be 48 Å using Barrett−Joyner−Halenda analysis of N_2 desorption (Figure S1A,B). The X-ray diffraction pattern of the particles, measured on a Rigaku Ultima IV X-ray diffractometer using Cu K_α radiation, matched that of monoclinic ZrO_2 (JCPDS 37−1484, Figure S1C).

Hexanoic and isopentanoic acid ketonization kinetics experiments were performed in a Dursan-coated (SilcoTek Coating Co.) stainless steel 4.7×10^{-3} m ID clamshell-heated packed-bed reactor described previously.[6,10] Briefly, gases fed using mass flow controllers (Brooks Instruments) were blended with liquids fed using a high-pressure liquid chromatography (HPLC) pump (Chromtech) at a heated inlet (200 °C), vaporizing the liquid feeds. Masses of liquids consumed were tracked by keeping liquid sources on mass balances (Mettler Toledo) and periodically recording mass decreases. The reaction mixture was flowed over a packed catalyst bed consisting of 0.05−1 g of ZrO_2 particles supported by a plug of glass wool and heated to 330−350 °C. Reactor effluent was passed through a liquid-cooled heat exchanger (2 °C), where nonvolatile species (acids, ketones, water) were condensed and subsequently collected in a knockout pot. No conversion of hexanoic acid was observed over glass wool alone, ensuring that all observed reactions occurred on the ZrO_2 catalyst surface. Liquid samples were collected from the knockout pot at 15−120 min intervals and quantified using a gas chromatograph (Agilent 7890) equipped with a PolyARC quantitative carbon detector (Activated Research Company). The gaseous ketonization product CO_2 was also monitored using an online NDIR detector (California Analytical Instruments, Inc.). During reactions, hexanoic acid (1.6×10^{4}-4.0×10^{-3} g s^{-1}) was fed to the reactor along with He sweep gas (0−0.6 $cm^3\ s^{-1}$ STP). Co-feeds were delivered either through a second mass-flow controller (CO_2) or a second HPLC pump (6-undecanone, deionized water). Lower flow rate limits of the HPLC pump limited the pressure of hexanoic acid delivered to the reactor as a pure liquid to slightly above 4 kPa. Thus, hexanoic acid was diluted in 4-heptanone (98%, Sigma-Aldrich) to deliver hexanoic acid at pressures lower than 4 kPa. Ketonization rates were assumed to be unaffected by 4-heptanone because 6-undecanone did not inhibit ketonization rates (*vide infra*). Total pressure during ketonization experiments was 81−83 kPa, ambient pressure in Golden, CO.

The mass balance (MB) on all recorded kinetic data points was 100 ± 10% and was defined as

$$\mathrm{MB} = \frac{\dot{m}_{\mathrm{acid,out}} + \dot{m}_{\mathrm{ketone,out}} + \dot{m}_{\mathrm{H_2O,out}} + \dot{m}_{\mathrm{CO_2,out}} + \dot{m}_{\mathrm{anhydride,out}}}{\dot{m}_{\mathrm{acid},in} + \dot{m}_{\mathrm{Cofeed,in}}} \quad (1)$$

Here, $\dot{m}_i$ is the mass flowrate of species i. Because our analytical setup precluded us from directly quantifying water and CO_2, we assumed that equivalent molar amounts of water and CO_2 accompanied ketone production and that equivalent molar amounts of water accompanied anhydride production (Scheme 2). Hexanoic acid ketonization kinetic data were recorded at differential conversion (128 of 135 kinetic data points recorded at <15% conversion, 103 recorded at <5% conversion) in conditions verified to be free of internal and external heat and mass transfer limits by the Mears[43] and Weisz-Prater[44] criteria (Section S2).

https://doi.org/10.1021/acs.iecr.1c04548
Ind. Eng. Chem. Res. 2022, 61, 2997−3010

Hexanoic acid reactions over ZrO_2 produced not only target product 6-undecanone (accompanied by water and CO_2) but also side product hexanoic anhydride (accompanied by water), as was observed by Wang and Iglesia.[27] We utilize the assumption of Wang and Iglesia of equilibrium between acids and anhydrides and accordingly quantify only 6-undecanone production, which comes from the equilibrated pool of hexanoic acid and hexanoic anhydride (Scheme 2, top and bottom right arrows).

Ketonization rate (r_{KET}) is quantified from the moles of 6-undecanone collected in a liquid sample (n_{Ketone}):

$$r_{KET} = \frac{n_{Ketone}}{m_{ZrO_2}\Delta t} \tag{2}$$

Here, m_{ZrO2} is the mass of catalyst in the packed bed reactor and Δt is the time interval between the time of collection of the previous and current liquid samples. Likewise, acid conversion is defined in terms of the amount of ketone formed:

$$X_{Acid} = \frac{2n_{Ketone}}{n_{Acid,fed}} \tag{3}$$

The fed amount of acid ($n_{Acid,fed}$) is quantified using the difference in the mass of the liquid source at the beginning and end of the sample collection interval.

We deconvoluted time-dependent catalyst deactivation from observed rates using a procedure analogous to that utilized by Harris, Bhan, and colleagues in studies of ethylene epoxidation,[45−49] allowing us to directly compare kinetic data collected at varied times on stream. The method is explained further in Section S3. An example of the decrease in rate over time in shown in Figure S2. This iteration of the kinetic model does not quantify deactivation over time, as this is a separate area of active study that we will address in a future publication.

2.2. Parameter Estimation Methods. We assume that hexanoic acid ketonization occurs via a Langmuir−Hinshelwood mechanism in which reaction occurs between two adsorbed hexanoic acid molecules. Ketonization rates are also modeled using a second-order Langmuir−Hinshelwood mechanism by Pham et al.[25] in a study of acetic, propionic, and butyric acid ketonization over Ru/TiO_2, Wang and Iglesia[27] in a study of acetic acid ketonization over TiO_2, and Gärtner et al.[26,37,38] in studies of butanoic, pentanoic, and hexanoic acid ketonization over $CeZrO_x$. Shylesh et al.[39] proposed a slightly different mechanism, in which two acid molecules adsorb to a single site before reacting, in studies of propionic acid ketonization over isolated Zr sites supported on SiO_2, but both this mechanism and the Langmuir−Hinshelwood mechanism are similar in that they suggest a gradual shift in the acid reaction order from 2 to 0 as acid pressure increases. The sequence of steps and the parameters used to represent each step are shown in eqs 4a−4e.

$$HA + * \rightleftharpoons HA^* \qquad K_{HA} \tag{4a}$$

$$2HA^* \rightarrow 6UD + CO_2 + H_2O + * \qquad k_{KET} \tag{4b}$$

$$6UD + * \rightleftharpoons 6UD^* \qquad K_{6UD} \tag{4c}$$

$$CO_2 + * \rightleftharpoons CO_2^* \qquad K_{CO2} \tag{4d}$$

$$H_2O + * \rightleftharpoons H_2O^* \qquad K_{H2O} \tag{4e}$$

In the mechanism, steps 4a and 4c−4e are assumed to be equilibrated, whereas step 4b is assumed to be irreversible. Here, HA is hexanoic acid and 6UD is 6-undecanone. We consider the net reaction to be irreversible because of the associated highly negative Gibbs free energy change (ΔG(350 °C, 1 bar) = −236 kJ/mol).[50]

Variation in the ketonization surface reaction rate constant (4b) with temperature was modeled using an Arrhenius-type dependence on a temperature-independent activation energy, E_A

$$k_{KET}(T) = k_{KET,0}e^{-E_A/RT} \tag{5}$$

whereas temperature dependence of the surface adsorption rate constants of adsorbed species A (K_A; 4a, 4c−4e) was modeled using a similar Arrhenius expression with a temperature-independent adsorption enthalpy ($\Delta H_{ads,A}$).

$$K_A(T) = K_{A,0}e^{-\Delta H_{ads,A}/RT} \tag{6}$$

In eqs 5 and 6, temperature (T) is in absolute units. The rate expression based on the mechanism in eqs 4a−4e is

$$r_{KET} = \frac{k_{KET}(T)(K_{HA}(T)P_{HA})^2}{(1 + K_{HA}(T)P_{HA} + K_{6UD}(T)P_{6UD} + K_{CO_2}(T)P_{CO_2} + K_{H_2O}(T)P_{H_2O})^2} \tag{7}$$

Prefactors, activation energies, and adsorption enthalpies were estimated from the kinetic data set in *MATLAB* using a Levenberg−Marquardt method (nlnfit function). Parameter errors were estimated using Bayesian methods via the *CheKiPEUQ Python* library.[51,52] All rates recorded during two of the temperature variation experiments (conditions ii and iii, see Section 3.1) were modeled with additional offsets to compensate for fixed random effects causing the rates measured at 350 °C in these experiments to be lower than those predicted by the model.[51]

2.3. Reactor Modeling Methods. The adiabatic packed-bed reactor model for hexanoic acid ketonization was written in *MATLAB* and solves the coupled system of differential equations describing the energy balance, mass balances, and pressure drop through the reactor (eqs 8−10) using ODE45. Reactor simulations satisfy or are close to satisfying the plug flow criterion for a packed-bed reactor ($Re_p = \frac{G}{\mu A_c} > 2000$, Re_p = particle Reynolds number). This assumption stipulates that temperature, species flow rates, and pressure vary only in the axial direction (varying catalyst mass, W) and is used in the energy and mass balances (eqs 8 and 9) as well as the Ergun equation (eq 10), which predicts the axial pressure profile.[53]

$$\frac{dT}{dW} = \frac{-\Delta H_{KET}\eta r_{KET}}{\widehat{C_p}\dot{m}_0} \tag{8}$$

$$\frac{dF_i}{dW} = \nu_i \eta r_{KET} \tag{9}$$

$$\frac{dP}{dW} = -\frac{1}{A_c\rho_p(1-\epsilon_{bed})}\left(\frac{G(1-\epsilon_{bed})}{\rho_0 D_p' \epsilon_{bed}^3}\left[\frac{150(1-\epsilon_{bed})\mu_{mixture}}{D_p'} + 1.75G\right]\right)\frac{P_0}{P}\frac{F_{Tot}}{F_{Tot,0}}\frac{T}{T_0} \tag{10}$$

https://doi.org/10.1021/acs.iecr.1c04548
Ind. Eng. Chem. Res. 2022, 61, 2997−3010

Table 1. Nomenclature and Parameter Values Used in the Reactor Model (eqs 8−15)

parameter symbol	meaning	value or formula
T, T_0	temperature, inlet temperature	350 °C inlet
W	catalyst mass	$W = A_c L_{Tube} \rho_{bulk}(1-\theta)(1-\varepsilon_{bed})$
A_c	cross-sectional area of tubular reactor	$A_c = \pi(D_{Tube}/2)^2$; D_{Tube} = 0.1524 m (6 in.)
L_{Tube}	reactor tube length	varies
ρ_{bulk}	bulk ZrO_2 density	5.68 g cm^{-3}[54]
θ	pellet void fraction	0.59625, from catalyst supplier
ε_{bed}	bed void fraction	0.41568, from catalyst supplier
D_p, L_p	diameter and length of extrudate particle	3.16×10^{-3} m and 5.44×10^{-3} m, from catalyst supplier
ΔH_{KET}	enthalpy of hexanoic acid ketonization, 350 °C	+5.308 kJ/mol, from the NIST Webbook and NIST/TRC Web Thermo Tables[50,55]
	specific heat capacity of mixture	mass fraction-weighted average of component heat capacities from the NIST/TRC Web Thermo Tables[50]
$\dot{m}_0$	total mass flow rate	1013 kg h^{-1}; based on ∼1000 kg h^{-1} industrial reactor throughput
F_i, F_{Tot}, $F_{Tot,0}$	molar flow rate of species i or all species (Tot), at inlet (Tot,0)	varies
P, P_0	pressure, inlet pressure	1−215 atm inlet, 1 atm outlet
ρ_p	ZrO_2 particle density	$\rho_p = \rho_{bulk}(1-\theta)$ = 2.29 g cm^{-3}
G	mass flux through reactor	$G = \frac{\dot{m}_0}{A_c}$
ρ_0	initial mass density of inlet stream	$\rho_0 = \frac{\dot{m}_0 P_0}{F_{Tot,0} R T_0}$
R	gas constant	8.314 J K^{-1} mol^{-1}
D_p'	sphericity-corrected particle diameter	$D_p' = \frac{(1.5 D_p^2 L_p)^{2/3}}{\left(\frac{D_p^2}{2} + D_p L_p\right)}$
$\mu_{Mixture}$	mixture viscosity	calculated from the Wilke formula[56] using component viscosities from the NIST/TRC Web Thermo Tables[50]
η	particle internal effectiveness factor	varies
c_i	molar concentration of species i	varies
r	pellet radius	between 0 and 1.58×10^{-3} m
N_i	molar flux of species i	varies
$D_{k,i}$	Knudsen diffusion coefficient of species i	$D_{k,i} = 0.97 r_{pore}\sqrt{\frac{T}{MW_i}}\frac{\theta}{\tau}$
r_{pore}	pore radius	48 Å (Section 2.1)
MW_i	molecular weight of species i	
τ	particle tortuosity	4; reasonable estimate[57]
x_i	mole fraction of species i	
$D_{i,j}$	binary diffusion coefficient of species i in species j	calculated using the Hirschfelder Equation[58]
R_i	net volumetric reaction rate of species i	$R_i = \nu_i r_{KET} \rho_{bulk}(1-\theta)$

Table 1 summarizes the nomenclature used in eqs 8−10 and contains typical values of physical parameters used in the reactor model. Boundary conditions for temperature, molar flow rates, and pressure are supplied at the inlet of the reactor and reactor size is determined by the length at which outlet pressure is atmospheric (1 atm).

The system in the reactor model has negligible external mass and heat transfer limitations (Section S2),[43] meaning that modeled particle surface concentrations and temperatures are equivalent to bulk values. System parameters also satisfy the Weisz−Prater criteria for internal heat transfer,[44] meaning that each particle has a uniform temperature (calculations in Section S2), but significant internal concentration gradients exist. At this condition, the internal effectiveness factors of the particles (η) will not be unity; they must be derived from internal pellet concentration profiles. Concentration profiles inside pellets are modeled using a combination of one-dimensional Stefan-Maxwell and Knudsen diffusion for each component i in the radial direction (eqs 11−12) using *MATLAB*'s BVP5C function. We model mass transport in the 2D pellet as only occurrent in the radial direction using this simplification, which we justify by noting that the ZrO_2 pellet radius is 3.3 times shorter than the length, ensuring that most mass flux will occur in the radial direction. We point out that Fickean diffusion is not applicable in this scenario because (i) the reaction mixture is not binary, (ii) the reaction mixture is not dilute, and (iii) the reaction creates three moles of gas for every two moles consumed, causing a net molar flux out of the particles.

$$\frac{dc_i}{dr} = -\frac{N_i}{D_{k,i}} + \sum_{j=1}^{n_{species}} \frac{x_i N_j - x_j N_i}{D_{i,j}} \tag{11}$$

$$\frac{dN_i}{dr} = R_i - \frac{N_i}{r} \tag{12}$$

Boundary conditions for eqs 11 and 12 are equivalent catalyst surface and fluid bulk concentrations at every point along the length of the reactor and zero flux through the center of the pellet:

$$c_i\left(r = \frac{D_p}{2}\right) = c_i(W) \tag{13}$$

https://doi.org/10.1021/acs.iecr.1c04548
Ind. Eng. Chem. Res. 2022, 61, 2997−3010

$$N_i(r = 0) = 0 \tag{14}$$

The nomenclature used in eqs 11−14 is explained in Table 1. Values of the internal effectiveness factor, η, are generated using the concentration profiles using eq 15 and calculated in *MATLAB* using a trapezoidal approximation based on computed radial concentration profiles.

$$\eta = \frac{\int_{V_{pellet}} r_i dV}{r_{i,surf} V_{pellet}} \tag{15}$$

As will be illustrated in Section 3.2, values of η are dependent only on temperature, pressure, and hexanoic acid conversion. Values of η in a grid of 9216 points in this three-dimensional parameter space were calculated by solving eqs 11−15 and the effectiveness factors were interpolated from this grid during reactor model operation to save computation time (Scheme S1).

Reactor simulations were performed assuming an influent flow rate of 1004 kg h^{-1} of hexanoic acid combined with 8.7 kg h^{-1} helium sweep gas (20 mol %) unless otherwise indicated. Helium was chosen to model as a sweep gas to emulate lab-scale reaction conditions. All reactor parameters are those outlined in Table 1 unless otherwise indicated. Transformation of VFA blendstocks into aviation fuel-range hydrocarbons (C_{8-16})[10] requires high overall process conversions and unreacted VFAs do not fit into this carbon number range. Thus, we aim to design a ketonization process that operates at near-complete (98%) acid conversion. Additionally, we seek to keep all reactants and products in the gas phase, which requires inlet pressures of less than ∼10 atm because the vapor pressure of 6-undecanone, the most condensable reactant or product, has a vapor pressure of 9.4 atm at the reference reaction temperature (350 °C).[50]

3. RESULTS AND DISCUSSION

3.1. Reaction Kinetics. Hexanoic acid was fed to the reactor at pressures between 0.8 and 75 kPa; ketonization rates at these conditions are shown in Figure 1A. The trend in rates with hexanoic acid pressure is congruent with our assumed Langmuir−Hinshelwood kinetics, as ketonization rates steeply increased from 0 to 10 kPa, then were constant at higher pressures, indicative of adsorbed hexanoic acid saturating active sites beyond 10 kPa. A similar trend in ketonization rates with acid pressure was observed by Gärtner et al. with of C_{4-6} acids over $CeZrO_x$[26,37,38] and Wang and Iglesia with acetic acid over TiO_2.[27]

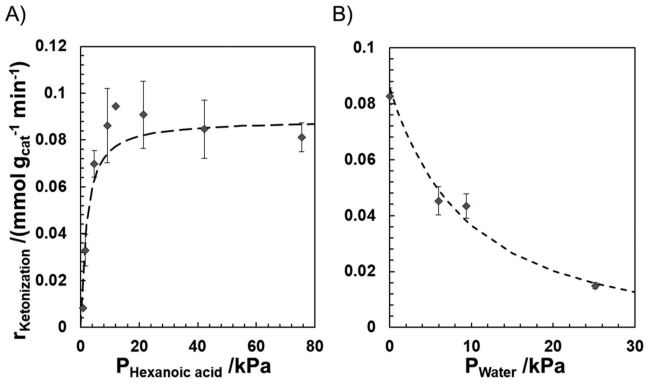

Figure 1. Hexanoic acid ketonization rates (measured, diamonds; modeled, dashed lines) over ZrO2 as a function of (A) hexanoic acid pressure and (B) water pressure. Error bars are standard deviations of 2−37 rate measurements at each condition. T = 350 °C, $P_{Hexanoic\ acid}$ = 0.8−75 kPa, P_{Water} = 0−25 kPa, m_{ZrO2} = 0.05−1 g. $X_{Hexanoic\ acid}$ is usually <10%.

We also assessed inhibition of ketonization rates by products water, CO_2, and 6-undecanone. Figure 1B shows that ketonization rates decline steeply with increasing cofed water pressure, indicating that water molecules compete with acids for adsorption on active sites. This finding is congruent with those of Pham et al.,[25,36] Gärtner et al.,[26,37,38] Fufachev et al.,[23] and Shylesh et al.,[39] who also report inhibition of ketonization rates by water. Water inhibition of ketonization rates can be explained by strong interactions of water molecules with Lewis acid and base sites, which have been implicated as the active sites for ketonization over oxides.[27,39] Water also inhibits the rates of other acid- or base-catalyzed reactions occurring over oxide catalysts, such as aldol condensations.[59,60]

Hexanoic acid ketonization rates were unaffected by cofeeds of 4−19 kPa CO_2 (Figure S3). Ketonization rates over TiO_2,[23,25,36] $CeZrO_x$,[37] and site-isolated ZrO_x/SiO_2[39] have been observed to be inhibited by CO_2, so we surmise that either the basic sites on our ZrO_2 catalysts do not absorb CO_2 strongly enough to significantly inhibit rates or that these sites are uninvolved in the rate-determining surface reaction. This result indicates that the value of K_{CO2} = 0 (eq 7). We were unable to quantify hexanoic acid ketonization rates (forming 6-undecanone) while cofeeding 6-undecanone and operating at differential conversion because expected produced amounts of 6-undecanone were more than an order of magnitude lower than the amount being cofed resulting in increased quantification uncertainty. This precluded us from directly quantifying the possible inhibition of hexanoic acid ketonization rates by 6-undecanone. Instead, we performed isopentanoic acid ketonization (43 kPa) and, after 244 min on stream, began cofeeding 21 kPa 6-undecanone. Figure S4 shows that the isopentanoic acid ketonization rate does not change upon the addition of 6-undecanone to the reaction mixture apart from the established deactivation trend with time on stream. This result indicates that 6-undecanone does not inhibit isopentanoic acid ketonization. We assume that all VFA ketonization processes have analogous mechanisms and conclude that hexanoic acid ketonization is likewise not inhibited by 6-undecanone, making K_{6UD} = 0 (eq 7). This result is contrary to findings of Gärtner et al.[26,37,38] and Pham et al.,[25,36] who observed inhibition of ketonization rates over solid oxides by ketones, but is harmonized with the findings of Baylon et al.,[61] who failed to observe aldol condensation of $C_{\geq 5}$ central ketones over a solid oxide catalyst, suggesting negligible interaction of these larger molecules with the catalyst surface.

The results of these kinetic experiments indicate that ketonization rates are described by only three temperature-dependent parameters, k_{KET}, K_{HA}, and K_{H2O}. We ran ketonization reactions at three sets of inlet pressures reflecting three important species pressure and surface coverage regimes to probe the temperature dependence of these parameters: (i) high hexanoic acid pressure ($\theta_{HA} \approx 1$; 42 kPa hexanoic acid), (ii) low hexanoic acid pressure ($\theta_{HA} \ll 1$; 0.8 kPa hexanoic acid), and (iii) high hexanoic acid and water pressures ($\theta_{HA} \approx \theta_{H2O} \approx 0.5$; 46 kPa hexanoic acid and 25 kPa water). We varied reaction temperature between 330 and 350 °C at each condition to determine the temperature dependence of each parameter. Ketonization rates are approximately zero order in

https://doi.org/10.1021/acs.iecr.1c04548
Ind. Eng. Chem. Res. 2022, 61, 2997−3010

acid pressure in regime (i) (Figure 1), meaning that the ketonization rate expression at these conditions simplifies to

$$r_{KET} = k_{KET}(T) \tag{16}$$

Variation in temperatures at this condition allowed for determination of E_A and $k_{KET,0}$. Similarly, at condition (ii), ketonization is positive order in acid pressure and the ketonization rate expression simplifies to

$$r_{KET} = \frac{k_{KET}(T)(K_{HA}(T)P_{HA})^2}{(1 + K_{HA}(T)P_{HA})^2} \tag{17}$$

If good estimates for E_A and $k_{KET,0}$ already exist, $\Delta H_{Ads,HA}$ and $K_{HA,0}$ can be determined in this regime. Finally, all relevant terms of the ketonization rate expression are significant at condition (iii).

$$r_{KET} = \frac{k_{KET}(T)(K_{HA}(T)P_{HA})^2}{(1 + K_{HA}(T)P_{HA} + K_{H_2O}(T)P_{H_2O})^2} \tag{18}$$

Temperature variation at this condition allows for estimation of $\Delta H_{Ads,H2O}$ and $K_{0,H2O}$ if good estimates for the remaining four parameters have been developed from the previous experiments. Figure S5 shows the effect of temperature variation on the rate at these conditions.

3.2. Parameter Estimation. Table 2 shows estimated values of the six parameters used in the hexanoic acid ketonization rate expression (eq 18). Estimated rates are shown as a function of hexanoic acid pressure in Figure 1A, water pressure in Figure 1B, and temperature in Figure S5. Location of all data near the $y = x$ line in the parity plot of predicted and observed rates (Figure 2) demonstrates that the model effectively captures our kinetic data.

Table 2. Hexanoic Acid Ketonization Kinetic Model Parameter Values and Errors

parameter	value
$k_{KET,0}$	$(4.1 \pm 1.8) \times 10^{12}$ mmol g_{ZrO2}^{-1} min^{-1}
E_A	160 ± 20 kJ mol^{-1}
$K_{HA,0}$	$(4.6 \pm 4.7) \times 10^{-10}$ kPa^{-1}
$\Delta H_{ads,HA}$	-112 ± 110 kJ mol^{-2}
$K_{H2O,0}$	0.0038 ± 0.0016 kPa^{-1}
$\Delta H_{ads,H2O}$	-34 ± 17 kJ mol^{-1}

Activation and adsorption energy parameters predicted by the model are within the range observed previously for ketonization reactions over similar catalysts. The activation energy we predict for the surface reaction step, 160 kJ/mol, is within the range of surface ketonization activation energies predicted previously, as the model developed by Gärtner et al.[37] predicts a hexanoic acid ketonization activation energy of 57.7 kJ mol^{-1} over $CeZrO_x$ and Pham et al.[25] predict activation energies of 156.4–220.0 kJ mol^{-1} for acetic, propionic, and butanoic acid ketonization over Ru/TiO_2. The breadth of this range indicates the variation in adsorptive and reactive properties even among solid oxide catalysts capable of facilitating ketonization, as well as changes in reactive properties between different VFAs. Adsorption enthalpy of hexanoic acid in our model, −112 kJ mol^{-1}, is also well within bounds predicted in previous studies, with Gärtner et al.[37] predicting an adsorption enthalpy of hexanoic acid on $CeZrO_x$ of −58.7 kJ mol^{-1} and both Wang and Iglesia[27] and Pham et al.[25] using adsorption enthalpies between −134 and −140 kJ mol^{-1} for C_{2-4} carboxylic acids over TiO_2 and Ru/TiO_2, respectively. The adsorption enthalpy of water in our model, −34 kJ mol^{-1}, is lower in magnitude than the value (−58 kJ mol^{-1}) reported by Lackner et al.[62] for water adsorption on ZrO_2 based on ultrahigh vacuum studies and density functional theory calculations and is also lower than the values derived from kinetic studies by Gärtner et al.[37] over $CeZrO_x$ (−96 kJ mol^{-1}) and Pham et al.[25] over Ru/TiO_2 (−82 kJ mol^{-1}). We ascribe this discrepancy and the substantial errors (≥50% of parameter values) on both $\Delta H_{ads,HA}$ and $\Delta H_{ads,H2O}$ to the fundamental shortcoming of approximating adsorption enthalpies as constant values independent of temperature or surface coverage changes. Wang and Iglesia[27] illustrate in their study of acetic acid ketonization using density functional theory calculations and kinetic analysis that multiple modes of adsorption of relevant surface species over solid oxide exists, and that enthalpies of these adsorptions are dependent on surface coverage and temperature. Nonetheless, the parameters in our model are physically feasible and quantitatively describe the kinetic trends observed in Section 3.1.

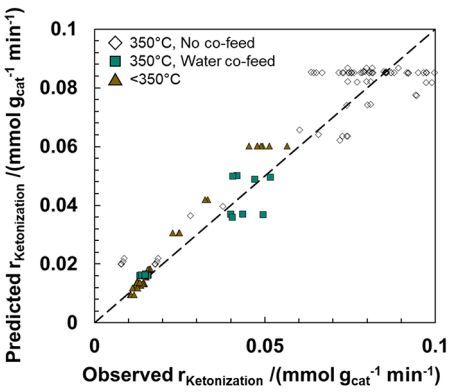

Figure 2. Parity plot of observed and predicted ketonization rates. Open diamonds are rates recorded at 350 °C with no cofeed and varied hexanoic acid pressure, teal squares are rates recorded at 350 °C with water cofeed, and brown triangles are rates recorded at temperatures other than 350 °C. Dotted line is $y = x$.

3.3. Packed-Bed Reactor Modeling and Reactor Design Principles. Formulation of the packed-bed reactor model hinged a great deal on the calculation of η, the internal effectiveness factor of ketonization in reactor pellets. We solved for η analytically as a function of overall pressure, temperature, and conversion at the outer boundary of the pellet, as outlined in Section 2.3. We note here that, since ketonization rate is a function of T, $P_{Hexanoic\ acid}$, and P_{Water}, and that both species pressures are functions of total pressure (P_{Total}) and conversion ($X_{Hexanoic\ acid}$), each set of T, P_{Total}, and $X_{Hexanoic\ acid}$ uniquely specifies a η value. Utilizing the relationships developed between Thiele modulus and internal effectiveness factor for integer reaction orders[63,64] is inadequate here because these expressions do not consider product inhibition, whereas our cofeeds of water (Figure 1B) demonstrate that product inhibition is significant during ketonization. Additionally, these relationships do not provide for reaction rate orders that change with reactant pressure, whereas Figure 1A shows that ketonization rates transition from second to zero order in hexanoic acid pressure as hexanoic acid pressure increases.

The decrease in ketonization rate and effectiveness factor caused by water inhibition inside catalyst extrudate pellets is demonstrated in Figure 3, which compares species pressures

https://doi.org/10.1021/acs.iecr.1c04548
Ind. Eng. Chem. Res. 2022, 61, 2997−3010

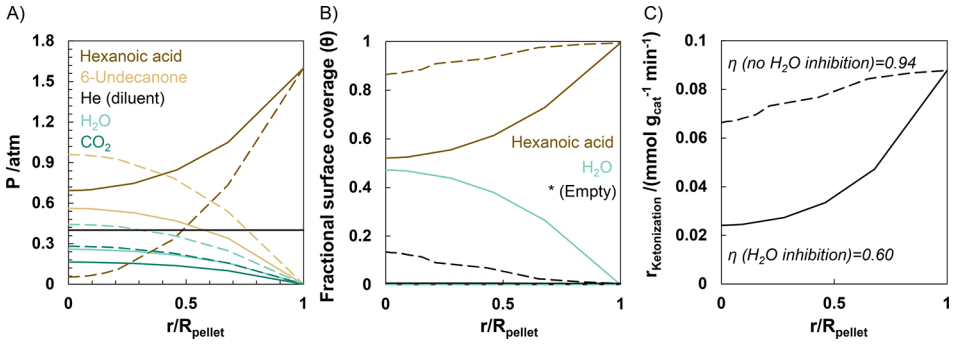

Figure 3. (A) Product, reactant, and diluent concentrations; (B) surface coverages; and (C) ketonization rates as a function of cylindrical pellet radius predicted by the ketonization reactor model. Solid lines represent quantities with water inhibition and dotted lines represent quantities without water inhibition. T = 350 °C; external pressures: 1.6 atm hexanoic acid, 0.4 atm He (diluent); R_{pellet} = 1.58 mm.

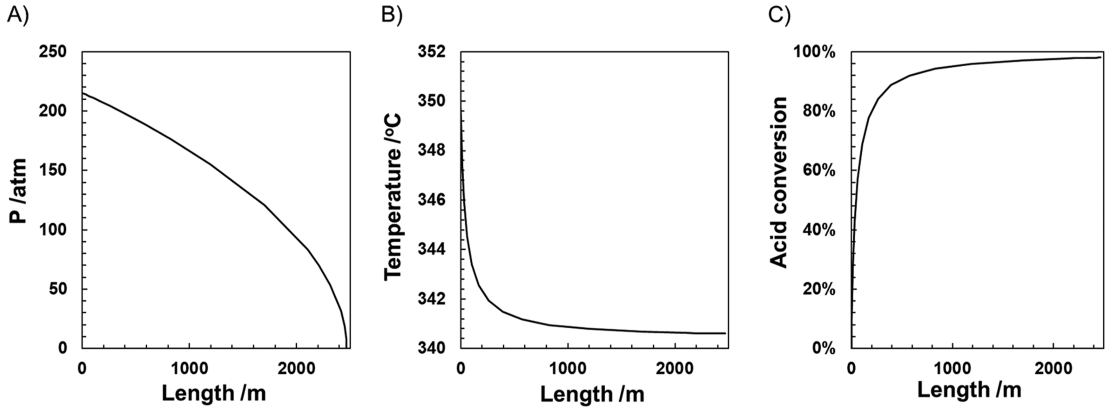

Figure 4. (A) Simulated pressure, (B) temperature, and (C) conversion profiles of a ketonization reactor (0.1524 m ID) running to 98% conversion as a function of axial reactor length.

(A), surface coverages (B), rates, and effectiveness factors (C) for ketonization in scenarios with (solid lines) and without (dashed lines; K_{H2O}=0) water inhibition. Figure 3A shows that hexanoic acid pressure decreases appreciably between the surface of the pellet and the interior, by 57% in the water inhibition scenario and by 97% in the non-water inhibition scenario. Despite the steeper decrease in concentration in the noninhibition case, the ketonization rate is higher in the noninhibition case than in the product inhibition case throughout the interior of the pellet (Figure 3C), with the effectiveness factor (η) close to unity (0.94) in the non-product inhibition case and markedly lower (0.60) in the product inhibition case. The phenomenon driving this difference is displacement of adsorbed hexanoic acid by water on the ZrO_2 surface, where surface coverages (θ) of water, hexanoic acid, and empty sites (*) are calculated using Langmuir isotherms derived from the ketonization rate expression (eq 18).

$$\theta_{HA} = \frac{K_{HA}P_{HA}}{1 + K_{HA}P_{HA} + K_{H_2O}P_{H_2O}} \quad (19a)$$

$$\theta_{H_2O} = \frac{K_{H_2O}P_{H_2O}}{1 + K_{HA}P_{HA} + K_{H_2O}P_{H_2O}} \quad (19b)$$

$$\theta_{*} = \frac{1}{1 + K_{HA}P_{HA} + K_{H_2O}P_{H_2O}} \quad (19c)$$

Figure 3B illustrates that hexanoic acid fractional surface coverage ($\theta_{Hexanoic\ acid}$) is near unity throughout the interior of the pellet (0.85−1) in the nonwater inhibition case, whereas the quantity decreases much more steeply, to 0.52, in the water inhibition case, despite the fact that the hexanoic acid pressure at the center of the pellet is ∼13 times higher in the water inhibition case than in the nonwater inhibition case. The strong adsorption of water on the catalyst in the water inhibition case is responsible for this difference, as θ_{H2O} at the center of the catalyst pellets is 0.47 in the product-inhibited case. This scenario illustrates the role of product inhibition in affirming that internal effectiveness factors must be calculated numerically.

Figure 4 shows the pressure, temperature, and conversion profiles of a packed-bed ketonization reactor running with the base case set of parameters and constraints outlined in Section 2.3 to 98% hexanoic acid conversion. Operating a reactor under these constraints would be infeasible because of the high length (2449 m) and inlet pressure (215 atm) utilized in the design. We considered four possible factors causing the base case reactor to require this intolerably large size and pressure drop: (i) internal diffusion limitations caused by large particle sizes, (ii) decrease in rate due to temperature drop in the adiabatic reactor, (iii) high pressures lowering reaction rates, and (iv) inhibition of ketonization rates by water. Perturbing parameters in the model concerning each of these scenarios (Section 3.3.1−3.3.4) led us to conclude that water inhibition is the primary driver governing reactor sizing.

3.3.1. Effect of Internal Diffusion Limitations on Reactor Design. We assessed the effect of internal diffusion limitations by decreasing the particle diameter in our effectiveness factor

https://doi.org/10.1021/acs.iecr.1c04548
Ind. Eng. Chem. Res. 2022, 61, 2997−3010

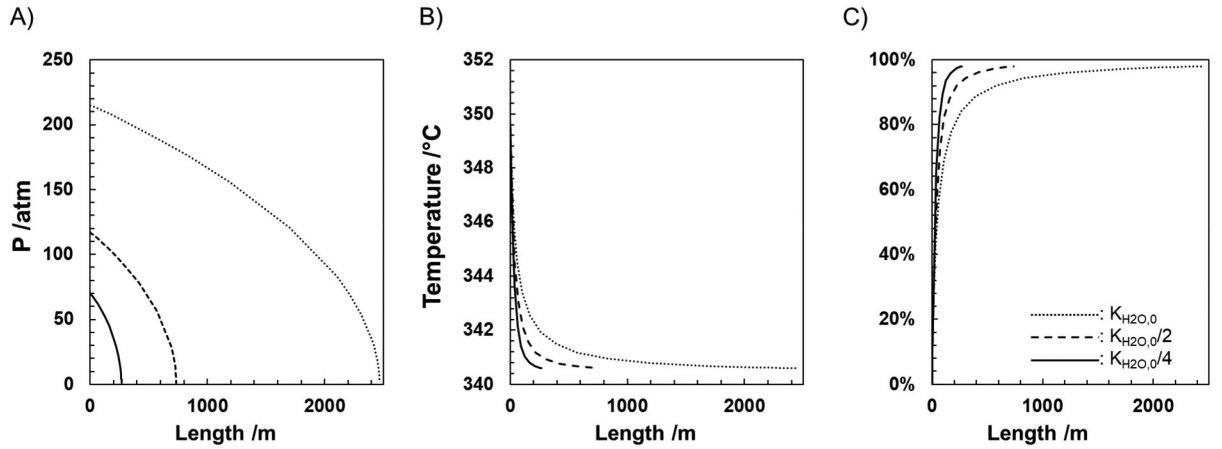

Figure 5. (A) Simulated pressure, (B) temperature, and (C) conversion profiles of a ketonization reactor (0.1524 m ID) running to 98% conversion as a function of axial reactor length with the originally measured water surface adsorption equilibrium constant compared to reactor performance with the water adsorption constant artificially halved and quartered.

calculation ($D_{p,diffusion}$) 10-fold, from 3.16 to 0.316 mm. This decrease was not accompanied by a change in particle size in the reactor-scale model. This change, then, altered only the conservative assumption taken in the base case model that the ZrO_2 pellets contain only mesoporosity (quantified via BET) and no macroporosity, the existence of which would need to be evaluated using tomography.[65] Any macroporosity would not alter the dimensions of particles on the reactor scale, but would decrease the size of the diffusion domains inside the pellets. Figure S6 shows the effect of decreasing the diffusion domain size 10-fold on catalyst internal effectiveness factor (A) and acid conversion (B) as a function of length. The figure shows that effectiveness factors of the particles are already close to one (η > 0.9) in the base reactor case (Figure S6A, dotted line), although decreasing the diffusion domain size increases effectiveness factor values to nearly unity (η > 0.999, Figure S6A, solid line). This change, however, only negligibly decreases the reactor length, from 2449 to 2448 m, and the conversion profiles across the reactor length are almost identical (Figure S6B). Thus, internal diffusion limitations do not significantly hinder the reactor performance and studying the macroporosity of ZrO_2 particles to determine if $D_{p,diffusion}$ is smaller than the macroscopic extrudate diameter will not influence projected sizing requirements of the ketonization reactor.

3.3.2. Effect of Temperature on Reactor Design. The temperature decrease over the adiabatic reactor length (9.5 °C) lowers the value of k_{KET} (eq 5), decreasing ketonization rates. We assessed the impact of this temperature drop by comparing the performance of the base case reactor to an isothermal reactor (dotted and solid lines respectively, Figure S7) and found that the necessary reactor length to achieve 98% conversion decreased only negligibly, by only ∼1.5%, in the isothermal case, from 2449 to 2412 m. We conclude on the basis of this simulation that temperature drop is not the driving factor behind the steep length and pressure requirements for the ketonization reactor.

3.3.3. Effect of Pressure on Reactor Design. Equation 18 shows that high pressures of hexanoic acid and water can inhibit ketonization rates, so we altered two separate reactor parameters, reactor diameter and flow rate, to simulate systems with lower overall pressure. Figure S8 shows the results of increasing the reactor diameter between 0.1524 (6 in., base case) and 0.6096 m (2 ft) while keeping the total inlet flow rate the same. This strategy does reduce the necessary reactor inlet pressure, decreasing it more than 50-fold, from 215 atm in the base case to 4.2 atm using a 0.6096 m diameter tube (Figure S8); the reactor length also decreases by a factor of more than 15, from 2449 to 159 m. The length decrease, however, is only a result of the corresponding increase in the reactor cross-sectional area. Figure S8 shows the catalyst mass (proportional to reactor volume) required for reactors of varying diameter and illustrates that required catalyst mass does not decrease, but instead increases by roughly 3%, from 60 333 to 62 161 kg, as reactor diameter increases from 0.1524 to 0.6096 m. We further discuss design consequences and trade-offs of employing wider (0.6096 m instead of 0.1524 m) reactors with minimal axial pressure gradients at the end of Section 3.4. We also modeled a reactor with identical diameter to the base case (0.1524 m) and one tenth of the base case inlet flow rates to simulate a scenario utilizing ten smaller reactors operating in parallel. Necessary inlet pressure for these smaller reactors dropped steeply in comparison to the base case, from 215 to 7.8 atm, similarly to the enlarged diameter designs. The total mass of catalyst required for ten such reactors, however, increased by ∼4% (from 60 333 to 62 791 kg) compared to the base case design. Both increasing reactor diameter and decreasing inlet flow rate by using multiple smaller reactors in parallel do reduce inlet reactor pressures, but catalyst mass and volume requirements slightly increase. This trade-off may be desirable in some cases, but decreasing the reactor pressure by increasing the tube diameter or running reactors in parallel is not a viable strategy to decrease both the axial pressure drop and the required reactor size.

3.3.4. Effect of Rate Inhibition by Water on Reactor Design. We showed previously the impact of water inhibition of ketonization rates (Section 3.1) and ZrO_2 pellet effectiveness factors (Figure 3) and demonstrate in Figure 5 the effect of water inhibition on overall reactor design. We simulated ketonization reactors with weaker water adsorption to the ZrO_2 surface by halving and quartering $K_{H2O,0}$ (Table 2). Figure 5 shows that this parameter, and therefore water inhibition, has an immense influence on the ketonization reactor design. Halving and quartering $K_{H2O,0}$ decreases the inlet pressure by 46 and 67% (from 215 to 117 and 70 atm, Figure 5A) and decreases the reactor length by 70 and 89%

https://doi.org/10.1021/acs.iecr.1c04548
Ind. Eng. Chem. Res. 2022, 61, 2997−3010

(from 2449 to 736 and 267 m, Figure 5) while maintaining 98% outlet acid conversion (Figure 5C). The temperature decrease from the reactor inlet to outlet is identical in all three cases (Figure 5B), further illustrating that the temperature decrease through these reactors is not the primary factor necessitating large reactor size and high inlet pressures. Designing a ketonization catalyst that adsorbs water more weakly than the ZrO_2 used here on its surface would, then, decrease the size requirements for a ketonization reactor, but this process is not straightforward.[66,67] Operating a ketonization reactor at a temperature higher than 350 °C may also be beneficial, as water may adsorb less strongly to the surface at higher temperatures. We show in the next section that reactor design alterations offer an alternative method for decreasing the size and pressure requirements for catalytic VFA ketonization reactors, an attractive outcome that would lower reactor capital costs.

3.4. Design Recommendations for Catalytic Ketonization Reactors. Figure 4C shows that hexanoic acid conversion increases steeply near the inlet of the reactor and then increases more and more slowly with increasing reactor length. In the base case, the final 720 m of the reactor, 30% of the total length, is required for raising the acid conversion from 97.1 to 98%. The first 586 m of the reactor, meanwhile, achieves over 92% hexanoic acid conversion using only 24% of reactor length. This example illustrates that product inhibition markedly increases reactor length requirements by depressing ketonization rates near the outlet of the reactor, where water pressure is the highest, suggesting that the required size and inlet pressure of a ketonization reactor can be sharply decreased by running the reactor at lower than 98% acid conversion.

Lowering the single-pass hexanoic acid conversion target of ketonization reactors results in dramatic decreases in length and influent pressure, although such reactors operating on their own would be insufficient to convert enough (98%) influent VFAs. Pushing target conversion down to 90% from 98% dramatically decreases the required inlet pressure and the length of a ketonization reactor (Figure 6A). The influent

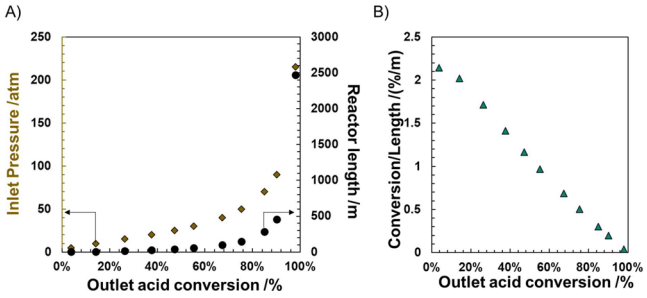

Figure 6. (A) Simulated inlet pressure (left axis) and reactor length (right axis) and (B) conversion per unit length as a function of conversion in a ketonization reactor (0.1524 m ID) running at various outlet acid conversions.

pressure drops 58%, from 215 to 90 atm, and the reactor length drops 82%, from 2449 to 451 m, when this conversion target is adjusted. Further relaxation of this conversion target decreases the reactor pressure and the length even more; running the ketonization reactor at 3.7% acid conversion would require only a length of 1.7 m with a 5 atm inlet pressure, decreasing the reactor length by more than 99.9% and the inlet pressure by more than 97% from the base case. Although the required reactor length and pressure should drop the accompanying lowering of target conversion, Figure 6B shows that the conversion per unit reactor length decreases monotonically as the target conversion increases. This illustrates that reactors operating at higher conversions utilize their lengths much less efficiently than those at lower conversions.

The infeasibility of operating single packed-bed ketonization reactors at near-complete conversion must be reconciled with the necessity of achieving high ketonization conversions, which are necessary to create ketone mixtures with long enough chain lengths to satisfy aviation fuel property requirements for biofuel blends after ketone hydrodeoxygenation.[10,68] The results presented in Figure 6 suggest that a reactor running at subcomplete (<98%) single-pass acid conversion would be optimal, and that water inhibition mars reactor performance. Several different reactor designs and configurations that periodically remove water from partially converted acid streams before the streams are reacted further could be deployed, including recycle, loop, and series reactors to remedy this issue. The separation of water from the rest of the partially reacted VFA, ketone, and CO_2 mixture at a reactor outlet could be accomplished in a straightforward manner by condensing the reactor effluent and separating the aqueous phase (water) from the organic phase (ketones and acids). Condensing the reactor effluent would also leave some CO_2 product in the gas phase and entrain some in condensed phases;[69] because CO_2 does not decrease ketonization rates (Section 3.1), dissolved CO_2 does not necessarily need to be eliminated from the organic phase until the final product purification. Recycle reactors would specifically require a more thorough purification step at the reactor outlet to separate ketone products (to be sent to storage or a hydrotreating reactor) and unreacted acids (to be sent back to the ketonization reactor influent). This could be accomplished by distillation if the reactor influent contains only single VFA species, as VFAs and their corresponding ketones have distinct boiling points (e.g., 205 °C for hexanoic acid and 228 °C for 6-undecanone).[55] However, novel separations techniques such as those developed to selectively extract VFAs from fermentation broth[70,71] will be needed to separate heterogeneous VFA mixtures from corresponding ketones, as the boiling point ranges of these mixtures overlap; C_2−C_8 VFA boiling points range from 118 to 237 °C and C_3−C_{15} ketone boiling points range from 56 to 291 °C.[55]

We show in Figure 7 axial pressure (A, B) and conversion (C) profiles in series reactors with interstage water separation (schematically represented in Figure 7D) achieving 98% hexanoic acid conversion compared to the base case reactor. Water is assumed to be separated perfectly from the effluent of each reactor stage with all other components fed to the next reactor. The inlet pressure and length of each reactor stage in a given design case is the same, excluding the final reactor, which has the minimum inlet pressure and length required to achieve 98% conversion. Figure 7 shows that even using two reactors drastically decreases both necessary inlet pressure (100 or 50 atm from 215 atm) and length (566 or 284 m from 2449 m) from the base case. Further increasing the number of reactor stages reduces cumulative length of combined reactors and input pressure; Figure 7 shows that nine reactors in series (eight using 10 atm inlet pressure and the ninth using 9 atm inlet pressure) necessitate only 63 m of total length, a more

https://doi.org/10.1021/acs.iecr.1c04548
Ind. Eng. Chem. Res. 2022, 61, 2997−3010

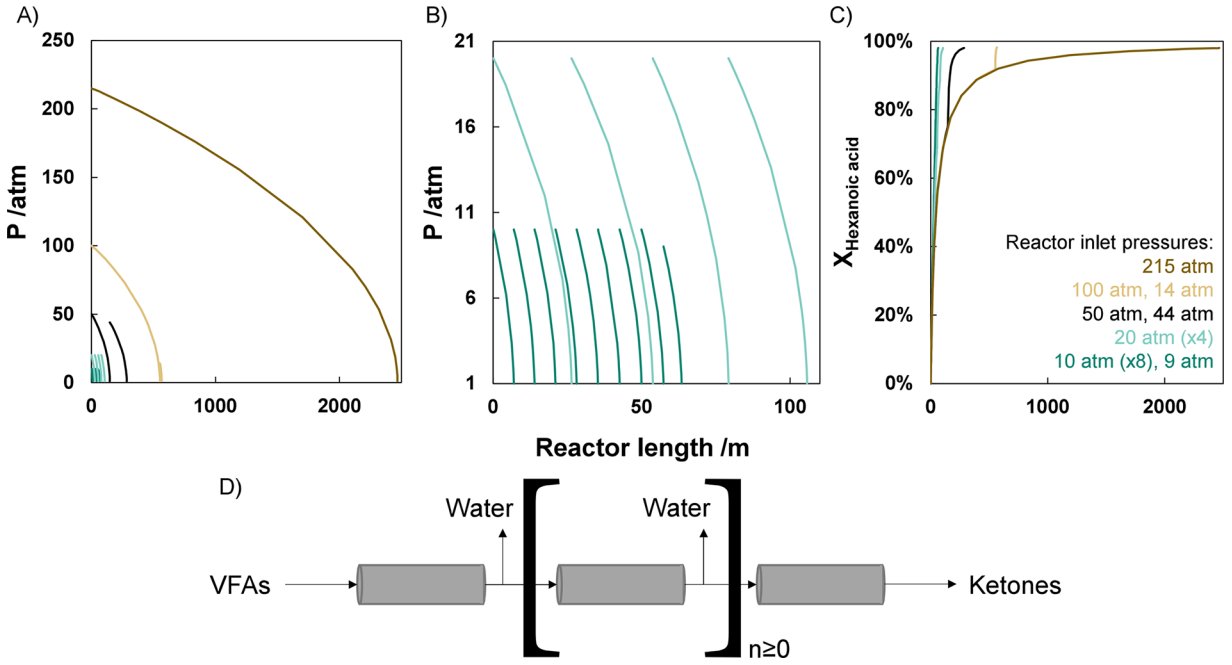

Figure 7. (A, B) Reactor pressure and (C) acid conversion in 1−9 hexanoic acid ketonization reactors operating in series with water removal between each reactor operating at 98% hexanoic acid conversion at the outlet of the final reactor. B is an inset of A. (D) Schematic representation of a VFA ketonization in series reactors with interstage water separation.

than 97% size decrease compared to the base reactor case. This analysis demonstrates the viability of series reactors for decreasing size and pressure requirements for industrial-scale hexanoic acid ketonization.

Figure S9 compares a case that also utilizes nine sequential reactors and larger-bore tubes (0.6096 m instead of 0.1524 m ID) to the minimum-size case explained in the previous example. The two reactor designs are compared on a basis of total catalyst mass utilized instead of reactor length since the tube diameters are no longer uniform. Figure S9A shows that increasing the tube size dramatically decreases pressure drop requirements, with inlet pressures of 1.025 atm (first eight reactors) and 1.012 atm (final reactor) necessary instead of 10 atm (first eight reactors) and 9 atm (final reactor) for the 0.1524 m ID reactor. However, this lower pressure also causes lower overall ketonization rates, as more of the reactor operates in a regime in which the ketonization pressure is low enough to cause rates to decrease with decreasing acid pressure (Section 3.1), necessitating 47% more ZrO_2 catalyst (2275 kg instead of 1550 kg). We also acknowledge that this 0.6096 m ID reactor will operate at Reynolds numbers between 125 and 176, below the plug flow regime at which the 0.1524 m ID reactor operates ($Re \geq 2000$). This will result in nonuniformities in residence time and radial temperature and concentration gradients, as well as possible particle-scale external heat- and mass-transfer limitations; these phenomena are beyond the scope of this study but would necessitate further increases in reactor size. Nonetheless, the trade-off of lower operating pressure for higher catalyst mass (and reactor size) requirements that accompanies the use of reactor tubes with diameters larger than 0.1524 m may be desirable in some cases.

Employment of recycle, loop, or series reactor configurations with outlet (recycle, loop) or interstage (series) water separations decreases the length and inlet pressure requirements of a carboxylic acid ketonization reactor. Optimal reactor configurations for carboxylic acid ketonization can be determined through the assessment of feasibility and energy requirements for separations procedures and process integration opportunities in tandem with careful technoeconomic analysis.

4. CONCLUSIONS

Volatile fatty acids can be upgraded to sustainable aviation fuel blends through catalytic ketonization followed by hydrodeoxygenation. We conducted a study of ketonization rates of a model VFA compound, hexanoic acid, at kinetically limited conditions over an industrially utilized ZrO_2 catalyst and found that (i) the rate is positive order in hexanoic acid pressure between 0 and ∼10 kPa, after which the rate is zero order in acid pressure, corroborating our assumption of ketonization occurring via a Langmuir−Hinshelwood surface reaction; and (ii) cofeeds of product water result in substantial rate decreases, whereas cofeeds of product CO_2 and 6-undecanone do not inhibit rates, signifying that only water competes with hexanoic acid for adsorption on the ZrO_2 surface. Parameters describing the ketonization surface reaction and the surface adsorption of hexanoic acid and water were fit using observed kinetic data to comprise a model that quantitatively describes observed ketonization rates at varied product and reactant pressures and temperatures. We used the kinetic model in a packed-bed reactor simulation incorporating ZrO_2 extrudate particle internal diffusion limitations and an axial pressure drop to simulate industrial-scale hexanoic acid ketonization. Rate inhibition by water was identified as the principal driver of reactor size and pressure drop. We recommend utilizing recycle, loop, or series reactors to carry out catalytic ketonization to high (98%) conversion and demonstrate that implementation of a series reactor configuration decreases the reactor size and pressure requirements of these systems compared to a single packed-bed reactor.

https://doi.org/10.1021/acs.iecr.1c04548
Ind. Eng. Chem. Res. 2022, 61, 2997−3010

■ ASSOCIATED CONTENT

Supporting Information

The Supporting Information is available free of charge at https://pubs.acs.org/doi/10.1021/acs.iecr.1c04548.

Catalyst characterization information, heat and mass-transport limitations calculations, and additional reaction and modeling data (PDF)

■ AUTHOR INFORMATION

Corresponding Author

Derek R. Vardon − *Catalytic Carbon Transformation and Scaleup Center, National Renewable Energy Laboratory, Golden, Colorado 80401, United States;* Present Address: Alder Fuels, Washington, DC 20007, United States; orcid.org/0000-0002-0199-4524; Email: dvardon@alderfuels.com

Authors

Jacob H. Miller − *Catalytic Carbon Transformation and Scaleup Center, National Renewable Energy Laboratory, Golden, Colorado 80401, United States;* orcid.org/0000-0002-0075-4430

Glenn R. Hafenstine − *Catalytic Carbon Transformation and Scaleup Center, National Renewable Energy Laboratory, Golden, Colorado 80401, United States;* Present Address: Honeywell FM&T, Kansas City, MO 64147, United States

Hannah H. Nguyen − *Catalytic Carbon Transformation and Scaleup Center, National Renewable Energy Laboratory, Golden, Colorado 80401, United States;* Present Address: CONTINUUS Pharmaceuticals, Woburn, MA 01801, United States

Complete contact information is available at: https://pubs.acs.org/10.1021/acs.iecr.1c04548

Notes

The authors declare the following competing financial interest(s): D.R.V. is Chief Technology Officer of Alder Fuels, LLC.

■ ACKNOWLEDGMENTS

We are grateful for the contributions of Drs. Nicholas E. Thornburg, M. Brennan Pecha, and Peter N. Ciesielski in formulating our experimental plan and kinetic model, Dr. Aditya Savara for helpful consultation on parameter estimation and error quantification, and James Stunkel, Alexander Rein, Gabriella Lahti, Dr. Wilson McNeary, and Stephen Tifft for experimental, revision, and characterization assistance. A portion of this research was conducted as part of the Opportunities in Biojet Project sponsored by the U.S. Department of Energy Office of Energy Efficiency and Renewable Energy and Bioenergy Technologies (BETO) and Vehicle Technologies Offices through Contract DE-AC36-08GO28308. A portion of this work was also conducted as part of the Chemical Catalysis for Bioenergy Consortium sponsored by BETO through Contract DE-AC36-08GO28308.

■ REFERENCES

(1) *Climate Change 2021: The Physical Science Basis: Contribution of Working Group I to the Sixth Assessment Report of the Intergovernmental Panel on Climate Change*; Cambridge University Press, 2021.

(2) Lee, D. S.; Fahey, D. W.; Skowron, A.; Allen, M. R.; Burkhardt, U.; Chen, Q.; Doherty, S. J.; Freeman, S.; Forster, P. M.; Fuglestvedt, J.; Gettelman, A.; De León, R. R.; Lim, L. L.; Lund, M. T.; Millar, R. J.; Owen, B.; Penner, J. E.; Pitari, G.; Prather, M. J.; Sausen, R.; Wilcox, L. J. The Contribution of Global Aviation to Anthropogenic Climate Forcing for 2000 to 2018. *Atmos. Environ.* **2021**, *244*, 117834.

(3) Zhang, L.; Butler, T. L.; Yang, B. Recent Trends, Opportunities and Challenges of Sustainable Aviation Fuel. In *Green Energy to Sustainability*; John Wiley & Sons, 2020; pp 85−110. DOI: 10.1002/9781119152057.ch5

(4) Bhatt, A. H.; Ren, Z.; Tao, L. Value Proposition of Untapped Wet Wastes: Carboxylic Acid Production through Anaerobic Digestion. *iScience* **2020**, *23* (6), 101221.

(5) Skaggs, R. L.; Coleman, A. M.; Seiple, T. E.; Milbrandt, A. R. Waste-to-Energy Biofuel Production Potential for Selected Feedstocks in the Conterminous United States. *Renewable and Sustainable Energy Reviews* **2018**, *82*, 2640−2651.

(6) Hafenstine, G. R.; Huq, N. A.; Conklin, D. R.; Wiatrowski, M. R.; Huo, X.; Guo, Q.; Unocic, K. A.; Vardon, D. R. Single-Phase Catalysis for Reductive Etherification of Diesel Bioblendstocks. *Green Chem.* **2020**, *22* (14), 4463−4472.

(7) Huo, X.; Huq, N. A.; Stunkel, J.; Cleveland, N. S.; Starace, A. K.; Settle, A. E.; York, A. M.; Nelson, R. S.; Brandner, D. G.; Fouts, L.; et al. Tailoring Diesel Bioblendstock from Integrated Catalytic Upgrading of Carboxylic Acids: A "Fuel Property First" Approach. *Green Chem.* **2019**, *21* (21), 5813−5827.

(8) Atasoy, M.; Owusu-Agyeman, I.; Plaza, E.; Cetecioglu, Z. Bio-Based Volatile Fatty Acid Production and Recovery from Waste Streams: Current Status and Future Challenges. *Bioresour. Technol.* **2018**, *268*, 773−786.

(9) Vardon, D. R.; Sherbacow, B. J.; Guan, K.; Heyne, J. S.; Abdullah, Z. Realizing "Net-Zero-Carbon" Sustainable Aviation Fuel. *Joule* **2022**, *6* (1), 16−21.

(10) Huq, N. A.; Hafenstine, G. R.; Huo, X.; Nguyen, H.; Tifft, S. M.; Conklin, D. R.; Stück, D.; Stunkel, J.; Yang, Z.; Heyne, J. S. Toward Net-Zero Sustainable Aviation Fuel with Wet Waste−Derived Volatile Fatty Acids. *Proc. Natl. Acad. Sci. U.S.A.* **2021**, *118* (13), e2023008118.

(11) Huq, N. A.; Huo, X.; Hafenstine, G. R.; Tifft, S. M.; Stunkel, J.; Christensen, E. D.; Fioroni, G. M.; Fouts, L.; McCormick, R. L.; Cherry, P. A.; et al. Performance-Advantaged Ether Diesel Bioblendstock Production by a Priori Design. *Proc. Natl. Acad. Sci. U.S.A.* **2019**, *116* (52), 26421−26430.

(12) Boekaerts, B.; Vandeputte, M.; Navaré, K.; Van Aelst, J.; Van Acker, K.; Cocquyt, J.; Van Caneyt, C.; Van Puyvelde, P.; Sels, B. F. Assessment of the Environmental Sustainability of Solvent-Less Fatty Acid Ketonization to Bio-Based Ketones for Wax Emulsion Applications. *Green Chem.* **2021**, *23* (18), 7137−7161.

(13) Schowanek, D.; Borsboom-Patel, T.; Bouvy, A.; Colling, J.; de Ferrer, J. A.; Eggers, D.; Groenke, K.; Gruenenwald, T.; Martinsson, J.; Mckeown, P.; Miller, B.; Moons, S.; Niedermann, K.; Pérez, M.; Schneider, C.; Viot, J.-F. New and Updated Life Cycle Inventories for Surfactants Used in European Detergents: Summary of the ERASM Surfactant Life Cycle and Ecofootprinting Project. *Int. J. Life Cycle Assess* **2018**, *23* (4), 867−886.

(14) Heyne, J.; Bell, D.; Feldhausen, J.; Yang, Z.; Boehm, R. Towards Fuel Composition and Properties from Two-Dimensional Gas Chromatography with Flame Ionization and Vacuum Ultraviolet Spectroscopy. *Fuel* **2022**, *312*, 122709.

(15) Holladay, J.; Abdullah, Z.; Heyne, J. S. *Sustainable Aviation Fuel: Review of Technical Pathways*; DOE/EE-2041 8292 ; Bioenergy Technologies Office (EE-3B), Office of Energy Efficiency and Renewable Energy (EERE), U.S. Department of Energy: Washington, DC, 2020.

(16) Yang, X.; Jenkins, R. W.; Leal, J. H.; Moore, C. M.; Judge, E. J.; Semelsberger, T. A.; Sutton, A. D. Hydrodeoxygenation (HDO) of Biomass Derived Ketones Using Supported Transition Metals in a Continuous Reactor. *ACS Sustainable Chem. Eng.* **2019**, *7* (17), 14521−14530.

(17) Pearlson, M.; Wollersheim, C.; Hileman, J. A Techno-Economic Review of Hydroprocessed Renewable Esters and Fatty Acids for Jet Fuel Production. *Biofuels, Bioprod. Bioref.* **2013**, *7* (1), 89−96.
(18) Boekaerts, B.; Sels, B. F. Catalytic Advancements in Carboxylic Acid Ketonization and Its Perspectives on Biomass Valorisation. *Applied Catalysis B: Environmental* **2021**, *283*, 119607−119607.
(19) Yu, Q.; Guo, Y.; Wu, X.; Yang, Z.; Wang, H.; Ge, Q.; Zhu, X. Ketonization of Propionic Acid on Lewis Acidic Zr-Beta Zeolite with Improved Stability and Selectivity. *ACS Sustainable Chem. Eng.* **2021**, *9*, 7982.
(20) Wang, X.; Ding, S.; Wang, H.; Liu, X.; Han, J.; Ge, Q.; Zhu, X. Applied Catalysis A, General Conversion of Propionic Acid and 3-Pentanone to Hydrocarbons on ZSM-5 Catalysts : Reaction Pathway and Active Site. *Applied Catalysis A, General* **2017**, *545* (April), 79−89.
(21) Gliński, M.; Kijeński, J.; Jakubowski, A. Ketones from Monocarboxylic Acids: Catalytic Ketonization over Oxide Systems. *Applied Catalysis A, General* **1995**, *128* (2), 209−217.
(22) Crisci, A. J.; Dou, H.; Prasomsri, T.; Roman-Leshkov, Y. Cascade Reactions for the Continuous and Selective Production of Isobutene from Bioderived Acetic Acid Over Zinc-Zirconia Catalysts. *ACS Catal.* **2014**, *4*, 4196−4200.
(23) Fufachev, E. V.; Weckhuysen, B. M.; Bruijnincx, P. C. A. Toward Catalytic Ketonization of Volatile Fatty Acids Extracted from Fermented Wastewater by Adsorption. *ACS Sustainable Chem. Eng.* **2020**, *8* (30), 11292−11298.
(24) Parida, K.; Mishra, H. K. Catalytic Ketonisation of Acetic Acid over Modified Zirconia. *J. Mol. Catal. A: Chem.* **1999**, *139* (1), 73−80.
(25) Pham, T. N.; Shi, D.; Resasco, D. E. Reaction Kinetics and Mechanism of Ketonization of Aliphatic Carboxylic Acids with Different Carbon Chain Lengths over Ru/TiO2 Catalyst. *J. Catal.* **2014**, *314*, 149−158.
(26) Gaertner, C. A.; Serrano-Ruiz, J. C.; Braden, D. J.; Dumesic, J. A. Catalytic Coupling of Carboxylic Acids by Ketonization as a Processing Step in Biomass Conversion. *J. Catal.* **2009**, *266* (1), 71−78.
(27) Wang, S.; Iglesia, E. Experimental and Theoretical Assessment of the Mechanism and Site Requirements for Ketonization of Carboxylic Acids on Oxides. *J. Catal.* **2017**, *345*, 183−206.
(28) Fufachev, E.; Weckhuysen, B.; Bruijnincx, P. Crystal Phase Effects on the Gas-Phase Ketonization of Small Carboxylic Acids over TiO2 Catalysts. *ChemSusChem2* **2021**, *14*, 2710.
(29) Albrecht, K.; Davidson, S.; Dagle, R.; Maddi, B.; Howe, D.; Cooper, A.; Lopez-Ruiz, J.; Panisko, E. *Final Report for the Project Characterization and Valorization of Aqueous Phases Derived from Liquefaction and Upgrading of Bio-Oils*; Office of Scientific and Technical Information, U.S. Department of Energy: Oak Ridge, TN, 2018.
(30) Davidson, S. D.; Lopez-Ruiz, J. A.; Flake, M.; Cooper, A. R.; Elkasabi, Y.; Tomasi Morgano, M.; Lebarbier Dagle, V.; Albrecht, K. O.; Dagle, R. A. Cleanup and Conversion of Biomass Liquefaction Aqueous Phase to C3−C5 Olefins over ZnxZryOz Catalyst. *Catalysts* **2019**, *9* (11), 923.
(31) Lopez-Ruiz, J. A.; Cooper, A. R.; Li, G.; Albrecht, K. O. Enhanced Hydrothermal Stability and Catalytic Activity of La x Zr y O z Mixed Oxides for the Ketonization of Acetic Acid in the Aqueous Condensed Phase. *ACS Catal.* **2017**, *7*, 6400.
(32) Ding, S.; Wang, H.; Han, J.; Zhu, X.; Ge, Q. Ketonization of Propionic Acid to 3-Pentanone over Ce x Zr 1- x O 2 Catalysts: The Importance of Acid-Base Balance. *Ind. Eng. Chem. Res.* **2018**, *57* (50), 17086−17096.
(33) Fufachev, E. V.; Weckhuysen, B. M.; Bruijnincx, P. C. A. Crystal Phase Effects on the Gas-Phase Ketonization of Small Carboxylic Acids over TiO2 Catalysts. *ChemSusChem* **2021**, *14* (13), 2710−2720.
(34) Almutairi, S. T.; Kozhevnikova, E. F.; Kozhevnikov, I. V. Applied Catalysis A, General Ketonisation of Acetic Acid on Metal Oxides : Catalyst Activity, Stability and Mechanistic Insights. *Applied Catalysis A, General* **2018**, *565*, 135−145.
(35) Lee, K.; Kim, M. Y.; Choi, M. Effects of Fatty Acid Structures on Ketonization Selectivity and Catalyst Deactivation. *ACS Sustainable Chem. Eng.* **2018**, *6*, 13035−13044.
(36) Pham, T. N.; Shi, D.; Resasco, D. E. Kinetics and Mechanism of Ketonization of Acetic Acid on Ru/TiO2 Catalyst. *Top. Catal.* **2014**, *57* (6−9), 706−714.
(37) Gaertner, C. A.; Serrano-Ruiz, J. C.; Braden, D. J.; Dumesic, J. A. Ketonization Reactions of Carboxylic Acids and Esters over Ceria-Zirconia as Biomass-Upgrading Processes. *Ind. Eng. Chem. Res.* **2010**, *49* (13), 6027−6033.
(38) Görtner, C. A.; Serrano-Ruiz, J. C.; Braden, D. J.; Dumesic, J. A. Catalytic Upgrading of Bio-Oils by Ketonization. *ChemSusChem* **2009**, *2* (12), 1121−1124.
(39) Shylesh, S.; Bettinson, L. A.; Aljahri, A.; Head-gordon, M.; Bell, A. T. Experimental and Computational Studies of Carbon − Carbon Bond Formation via Ketonization and Aldol Condensation over Site-Isolated Zirconium Catalysts. *ACS Catal.* **2020**, *10*, 4566−4579.
(40) Pulido, A.; Oliver-Tomas, B.; Renz, M.; Boronat, M.; Corma, A. Ketonic Decarboxylation Reaction Mechanism: A Combined Experimental and DFT Study. *ChemSusChem* **2013**, *6* (1), 141−151.
(41) Bamberger, E. Notiz Über Das Verhalten von Essigsäureanhydrid Bei Hoher Temperatur. *Berichte der deutschen chemischen Gesellschaft* **1910**, *43* (3), 3517−3520.
(42) Pham, T. N.; Sooknoi, T.; Crossley, S. P.; Resasco, D. E. Ketonization of Carboxylic Acids: Mechanisms, Catalysts, and Implications for Biomass Conversion. *ACS Catal.* **2013**, *3* (11), 2456−2473.
(43) Mears, D. E. Diagnostic Criteria for Heat Transport Limitations in Fixed Bed Reactors. *J. Catal.* **1971**, *20* (2), 127−131.
(44) Weisz, P. B.; Prater, C. D. Interpretation of Measurements in Experimental Catalysis. *Adv. Mater.* **1954**, *6*, 143−196.
(45) Harris, J. W.; Bhan, A. Kinetics of Chlorine Deposition and Removal over Promoted Silver Catalysts during Ethylene Epoxidation. *J. Catal.* **2019**, *380*, 318−331.
(46) Harris, J. W.; Bhan, A. Moderation of Chlorine Coverage and Ethylene Epoxidation Kinetics via Ethane Oxychlorination over Promoted Ag/α-Al2O3. *J. Catal.* **2018**, *367*, 62−71.
(47) Harris, J. W.; Herron, J. A.; DeWilde, J. F.; Bhan, A. Molecular Characteristics Governing Chlorine Deposition and Removal on Promoted Ag Catalysts during Ethylene Epoxidation. *J. Catal.* **2019**, *377*, 378−388.
(48) Chen, C.-J.; Harris, J. W.; Bhan, A. Kinetics of Ethylene Epoxidation on a Promoted Ag/α-Al 2 O 3 Catalyst-The Effects of Product and Chloride Co-Feeds on Rates and Selectivity. *Chem.—Eur. J.* **2018**, *24*, 12405−12415.
(49) Iyer, K. R.; Bhan, A. Interdependencies Among Ethylene Oxidation and Chlorine Moderation Catalytic Cycles Over Promoted Ag/α-Al2O3 Catalysts. *ACS Catal.* **2021**, *11*, 14864−14876.
(50) Kroenlein, K.; Muzny, C. D.; Kazakov, A. F.; Diky, V.; Chirico, R. D.; Magee, J. W.; Abdulagatov, I.; Frenkel, M. *NIST/TRC Web Thermo Tables (WTT)*; Thermodynamics Research Center (TRC) Thermophysical Properties Division: Boulder, CO, 2021.
(51) Savara, A.; Walker, E. A. CheKiPEUQ Intro 1 : Bayesian Parameter Estimation Considering Uncertainty or Error from Both Experiments and Theory. *ChemCatChem* **2020**, *12*, 5385−5400.
(52) Walker, E. A.; Ravisankar, K.; Savara, A. CheKiPEUQ Intro 2: Harnessing Uncertainties from Data Sets, Bayesian Design of Experiments in Chemical Kinetics**. *ChemCatChem.* **2020**, *12* (21), 5401−5410.
(53) Rawlings, J. B.; Ekerdt, J. G. *Chemical Reactor Analysis and Design Fundamentals*, 2nd ed.; Nob Hill Publishing: Madison, WI, 2012.
(54) *CRC Handbook of Chemistry and Physics*, 95th ed.; Haynes, W., Lide, D., Bruno, T., Eds.; CRC Press: Boca Raton, FL, 2014.
(55) Linstrom, P. J.; Mallard, W. G. *NIST Chemistry WebBook, NIST Standard Reference Database Number 69*; Linstrom, P. J., Mallard, W.

https://doi.org/10.1021/acs.iecr.1c04548
Ind. Eng. Chem. Res. 2022, 61, 2997−3010

G., Eds.; National Institute of Standards and Technology: Gaithersburg, MD, 2021.
(56) Wilke, C. R. A Viscosity Equation for Gas Mixtures. *J. Chem. Phys.* **1950**, *18* (4), 517−519.
(57) Davis, M. E.; Davis, R. J. *Fundamentals of Chemical Reaction Engineering*; Pearson: London, 2003; p 239.
(58) Welty, J. R.; Wicks, C. E.; Wilson, R. E.; Rorrer, G. L. *Fundamentals of Momentum, Heat, and Mass Transfer*, 5th ed.; John Wiley & Sons: Hoboken, NJ, 2008.
(59) Zhang, H.; Ibrahim, M. Y. S.; Flaherty, D. W. Aldol Condensation among Acetaldehyde and Ethanol Reactants on TiO2: Experimental Evidence for the Kinetically Relevant Nucleophilic Attack of Enolates. *J. Catal.* **2018**, *361*, 290−302.
(60) Rorrer, J. E.; Toste, F. D.; Bell, A. T. Mechanism and Kinetics of Isobutene Formation from Ethanol and Acetone over ZnxZryOz. *ACS Catal.* **2019**, *9* (12), 10588−10604.
(61) Baylon, R. A. L.; Sun, J.; Martin, K. J.; Venkitasubramanian, P.; Wang, Y. Beyond Ketonization: Selective Conversion of Carboxylic Acids to Olefins over Balanced Lewis Acid-Base Pairs. *Chem. Commun.* **2016**, *52* (28), 4975−4978.
(62) Lackner, P.; Hulva, J.; Kock, E.-M.; Mayr-Schmolzer, W.; Choi, J. I. J.; Penner, S.; Diebold, U.; Mittendorfer, F.; Redinger, J.; Klotzer, B.; Parkinson, G. S.; Schmid, M. Water Adsorption at Zirconia: From the ZrO2(111)/Pt3Zr(0001) Model System to Powder Samples. *Journal of Materials Chemistry A* **2018**, *6*, 17587−17601.
(63) Fogler, H. S. *Elements of Chemical Reaction Engineering*, 1st ed.; Prentice-Hall: Englewood Cliffs, NJ, 1986.
(64) Froment, G. F.; Bischoff, K. B. *Chemical Reactor Analysis and Design*, second ed.; John Wiley & Sons: Hoboken, NJ, 1990.
(65) Pecha, M. B.; Iisa, K.; Griffin, M.; Mukarakate, C.; French, R.; Adkins, B.; Bharadwaj, V. S.; Crowley, M.; Foust, T. D.; Schaidle, J. A.; Ciesielski, P. N. Ex Situ Upgrading of Pyrolysis Vapors over PtTiO 2 : Extraction of Apparent Kinetics via Hierarchical Transport Modeling. *Reaction Chemistry & Engineering* **2021**, *6* (1), 125−137.
(66) Morterra, C.; Cerrato, G.; Bolis, V. Lewis and Brønsted Acidity at the Surface of Sulfate-Doped ZrO2 Catalysts. *Catal. Today* **1993**, *17* (3), 505−515.
(67) Wiwattanapongpan, J.; Mekasuwandumrong, O.; Chaisuk, C.; Praserthdam, P. Effect of Dopants on the Properties of Metal-Doped Zirconia Prepared by the Glycothermal Method. *Ceram. Int.* **2007**, *33* (8), 1469−1473.
(68) *ASTM-D7566 (20b) Standard Specification for Aviation Turbine Fuel Containing Synthesized Hydrocarbons*; ASTM International: West Conshohocken, PA, 2020.
(69) Marcus, Y. Solubility Parameter of Carbon Dioxide—An Enigma. *ACS Omega* **2018**, *3* (1), 524−528.
(70) Saboe, P. O.; Manker, L. P.; Michener, W. E.; Peterson, D. J.; Brandner, D. G.; Deutch, S. P.; Kumar, M.; Cywar, R. M.; Beckham, G. T.; Karp, E. M. In Situ Recovery of Bio-Based Carboxylic Acids. *Green Chem.* **2018**, *20* (8), 1791−1804.
(71) Carvajal-Arroyo, J. M.; Andersen, S. J.; Ganigué, R.; Rozendal, R. A.; Angenent, L. T.; Rabaey, K. Production and Extraction of Medium Chain Carboxylic Acids at a Semi-Pilot Scale. *Chemical Engineering Journal* **2021**, *416*, 127886.

https://doi.org/10.1021/acs.iecr.1c04548
Ind. Eng. Chem. Res. 2022, 61, 2997−3010